RSC Advances

PAPER

View Article Online
View Journal | View Issue

Cite this: *RSC Adv.*, 2020, **10**, 4232

Cross-linking of poly(dimethylaminoethyl methacrylate) by phytic acid: pH-responsive adsorbent for high-efficiency removal of cationic and anionic dyes

Wenbo Liu,[a] Rui Hu,[a] Yanke Li,[a] Yangze Huang,[a] Yixi Wang,[a] Zhong Wei,[a] Erlei Yu *[ab] and Xuhong Guo *[ab]

A new high-efficiency adsorbent for cationic and anionic dyes named PAGD was synthesized *via* polymerization of dimethylaminoethyl methacrylate by employing glycidyl-methacrylate-modified phytic acid as a cross-linker. The experiment demonstrated that PAGD is pH-sensitive, and the maximum adsorption capacities of anionic dye Reactive Red 24 (RR24) and cationic dye Fuchsin Basic (FB) were 1871.23 and 482.54 mg g^{-1}, respectively. To the best of our knowledge, there has been no previous report on a dye adsorbent possessing an adsorption capacity of over 465 mg g^{-1} for RR24. The excellent adsorption abilities toward RR24 are due to the introduced phytic acid groups, which could promote protonation of tertiary amine groups under acid pH conditions. Moreover, PAGD is able to selectively remove RR24 in a mixed solution of cationic dye and RR24. The adsorption isotherms and kinetics of PAGD fit well with the Langmuir isotherm and pseudo-second-order kinetic model, respectively. These results imply that PAGD is a promising adsorbent for removal of both cationic and anionic dyes.

Received 12th November 2019
Accepted 19th January 2020

DOI: 10.1039/c9ra09391e

rsc.li/rsc-advances

1. Introduction

Nowadays, with fast economic and technological development, wastewater pollution of organic dyes in the industry has become a critical issue of widespread concern.[1,2] Most of these dyes are harmful to ecosystems[3] owing to their non-degradability and toxicity.[4] Various techniques, for example, adsorption, membrane separation, flocculation, electrolysis, oxidation, and electro-coagulation, have been used to treat dye pollution.[5–10] Among the above-mentioned methods, adsorption is an advanced and prospective technique due to its low cost, simple operation, and high selectivity, which will not cause secondary pollution after removing pollutants from industrial wastewater.[11] Activated carbon is the most commonly adopted adsorbent for the treatment of dye waste now, but traditional activated carbon has the disadvantages of low efficiency and high cost. Many researchers have reported different physical or chemical treatments of primary substance adsorbents to increase their adsorption capacity.[12] However, materials with selectivity and a high dye-removal capacity are rare, and it has become quite necessary to explore several new types of inexpensive, higher adsorption-capacity, and exactly high-selectivity or pH-sensitive adsorbent material for particular dyes.[13]

Phytic acid (PA), known as inositol hexakisphosphate, which is abundant in many plant systems such as legumes, seeds, spores, and grains, is a natural and eco-friendly compound containing six phosphonic acids.[14] Recently, PA has begun to attract increasing interests for its highly effective abilities to remove dyes from wastewater.[15] Cai *et al.* synthesis a PA modified magnetic $CoFe_2O_4$ composite and found that the composites could selective adsorb methylene blue and congo red, which attributes to the synergistic effect of ion exchange and electrostatic interaction.[16] Zhao *et al.* prepared a three-dimensional poly acrylamide–phytic acid–polydopamine hydrogel that can be served as reusable adsorbent with high efficiency for removal of both anionic and cationic dyes. The analysis indicates that the dyes are adsorbed on the hydrogel through the strong π–π stacking and anion–cation interaction and can be easily removed from water regenerated by adjusting solution pH values.[17] You *et al.* proposed the preparation of PA-modified wheat straw to enhance the adsorption capacity of methylene blue dye, and these results indicated that PA-WS can be reused effectively and was a promising adsorbent for the removal of cationic dyes.[18] Owing to a negatively charged phosphate group, PA can adsorb cationic dyes and provides a variety of possible cross-linking sites.

2-(Dimethylamine)ethyl methacrylate (DMAEMA) monomers are often used to modify some polymeric adsorbents to enhance the adsorption of anions for its tertiary amino groups and pH-

[a]*Key Laboratory for Green Process of Chemical Engineering of Xinjiang Bingtuan, School of Chemistry and Chemical Engineering, Shihezi University, Shihezi 832003, P. R. China. E-mail: yuerlei120@163.com*

[b]*State Key Laboratory of Chemical Engineering, East China University of Science and Technology, Shanghai 200237, China. E-mail: guoxuhong@ecust.edu.cn*

sensitivity. Salama *et al.* reported a carboxymethyl cellulose-*g*-poly[2-(dimethylamino)ethyl methacrylate] hydrogel that possessed high maximum adsorption capacity (1825 mg g^{-1}) of methyl orange.[19] Karthika *et al.* used gellan gum-grafted poly[(2-dimethylamino)ethyl methacrylate] hydrogel to adsorb methyl orange in aqueous solution.[20] Krishnappa *et al.* prepared hydrocoagulation by simultaneous grafting and crosslinking of Karaya gum by microwave irradiation using DMAEMA and *N*,*N*′-methylene-bis-acrylamide. The gum is used to adsorb anionic and cationic dyes from wastewater and the graft copolymer was found to be pH and temperature responsive in nature.[21] From previous studies we can see that poly(DMAEMA) is a promising absorbent with pH responsive behaviour. The combination of PA and GMA may result in adsorbent material with high adsorption capacity and pH-sensitive properties to particular dyes. However, to the best of our knowledge, there are no reports on the cross-linking of poly(DMAEMA) by PA.

In this work, we modified PA with glycidyl methacrylate to obtain several unsaturated double bonds, and then cross-linked DMAEMA to prepare a new absorbent, PAGD, which could exhibit pH-sensitivity in both of cationic and anionic dyes. The influence factors were systematically discussed, including contact time, pH, temperature, adsorbent dosage, and dye concentration. In addition, kinetic and adsorption isotherms were used for intermittent adsorption experiments to evaluate their adsorption properties. The recycling of PAGD was assessed through five iterations of dye adsorption–desorption.

2. Experimental

2.1 Materials

PA (70 wt% in H_2O) was provided from Shanghai Aladdin Chemistry Reagent Co. Ltd. Fuchsin Basic (FB), Reactive Red 24 (RR24), methylene blue (MB), GMA and DMAEMA were purchased from Shanghai Macklin Biochemical Co. Ltd. (Shanghai, China). The information of FB and RR24 are shown in Table 1. Potassium peroxydisulfate (KPS) was obtained from Shengao Chemical Co. Ltd. (Tianjing, China). Analytically pure reagents of HCl and NaOH were bought from commercial sources without further treatment.

2.2 Synthesis of PAGD absorbent

Firstly, 1 g PA and 0.9045 g GMA were added in a 10 mL round flask. The reaction was kept at room temperature with stirring until the acid value was constant. Secondly, 2 g DMAEMA and 20 mg KPS were dissolved in 20 mL water and added into above solution under N_2 atmosphere at 70 °C with a magnetic stirring (200 rpm). The crosslinking product was obtained until complete gelation and cut into small pieces and washed thoroughly with ethanol and distilled water three times. Finally, the PAGD absorbent was obtained after being washed three times with ethanol and distilled water and freeze-dried at −50 °C for 24 h. The synthesis of PAGD was illustrated in Scheme 1.

2.3 Characterization

Fourier-transform infrared (FT-IR) spectra of the samples were recorded to qualitative analysis the functional groups of PAGD with an IS10 FTIR spectrophotometer (Nicolet, USA). Scanning electron microscopy (SEM) (SU8020, Hitachi, Japan) was used to characterize the morphology and cross-network structure of the adsorbent. ^{13}C NMR spectra were obtained on a JNM-ECZ600R spectrometer equipped with a broadband probe and ^{13}C-detected spectra were acquired using 50 scans. X-ray diffraction (XRD) was performed using Bruker AXS, D8 Advance with Cu Kα radiation ($\lambda = 0.15406$ nm) in the 2θ range from 20° to 80°. The concentrations of dyes were investigated by UV-vis spectroscopic (UV-6100S). A pH meter (PHB-4, Shanghai, China) was used to measure the pH value of aqueous solution.

2.4 Adsorption process

All adsorption batch experiments were carried out in 100 mL flasks with 50 mL dye solution (100 mg L^{-1}), which were stirred at 200 rpm in a thermostatic shaker. The adsorption capacity Q_e (mg g^{-1}) and removal rate (R, %) were given as eqn (1) and (2):

$$Q_e = \frac{(C_0 - C_e)V}{M} \quad (1)$$

$$R(\%) = \frac{100(C_0 - C_e)}{C_0} \quad (2)$$

where C_0 (mg L^{-1}) and C_e (mg L^{-1}) mean the initial concentration and equalized concentration respectively; V (L) and M (g) represent solution volume and adsorbent quality, respectively.

Kinetic experiments were implemented at 30 °C. The adsorption isotherm was studied by adding 50 mg of PAGD in 50 mL dye solution for 120 min to achieve adsorption equilibrium. The dye solution was filtered through a filter paper and analyzed with UV-vis spectrophotometer.

2.5 Regeneration

50 mg PAGD were soaked into 50 mL aqueous solution of dye (100 mg L^{-1}). When the equilibrium was achieved, the adsorbent was separated and placed in 50 mL distilled water for desorption. The PAGD for adsorption–desorption process were duplicated five times at room temperature. The desorption ratio (D%) was computed according to eqn (3):

$$D(\%) = \frac{C_d V_d}{(C_0 - C_e)V_i} \times 100\% \quad (3)$$

where C_d (mg L^{-1}) is the dye desorption solution concentration; V_d (mL) and V_i (mL) are the volume of the desorption and adsorption solution, respectively; C_0 (mg L^{-1}) and C_e (mg L^{-1}) are the initial and equilibrium concentration of dye among the adsorption process.

3. Results and discussion

3.1 Synthesis and characterization of PAGD

Fourier-transform infrared (FTIR) spectroscopy was used to confirm the structure of PAGD absorbent, and the result is shown in Fig. 1a. The spectrum shows peaks at 1729, 2827, and 2779 cm^{-1}, indicating the ester stretching carbonyl and the shearing chatter of –CH_2– and –CH_3 groups, respectively.[22,23]

Table 1 Classification and molecular structure of the selected dyes

Name	Dye category	Maximum wavelength	Molecular structure
Reactive Red 24 (RR24)	Anionic	533 nm	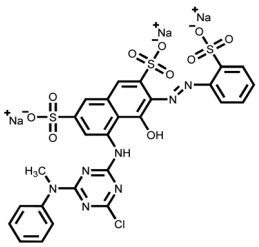
Fuchsin Basic (FB)	Cationic	543 nm	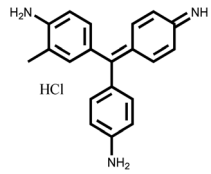

Moreover, the absorption band at approximately 1239 cm^{-1} is related to C–N vibration.[18] The peak at 1648 cm^{-1} is due to the flexural oscillation of –OH.[24] The additional peaks at 1154 and 1058 cm^{-1} were consistent with the extending chatter of P=O and O–P–C in PA.[25,26] The peaks at 846 and 986 cm^{-1} can be ascribed to in-plane winding of PO_4^{3-} and the stretching vibration of O–P–O.[27] The wide peaks appearing at 3426 and 2957 cm^{-1} correspond to the stretching vibrations of –OH and C–H, respectively.[28,29] The chemical structure of PAGD was characterized by solid-state ^{13}C NMR (Fig. 1b). In the ^{13}C NMR spectrum, peaks at 207 ppm represent the carbonyl carbon; peaks at 138 ppm,148 ppm and 49 ppm represent the methine carbon and –C–N– in DMAEMA, respectively; peaks at 128 ppm represent the methyl carbon in GMA.[30–32] These results indicate that the PAGD was successfully synthesized. It can also be confirmed by scanning electron microscopy (SEM) (Fig. 1c and d), before and after adsorption of the adsorbent, that the PAGD adsorbent is a porous network cross-linked structure. One can see from the X-ray-diffraction (XRD) pattern (Fig. 1e) that the adsorbent PAGD has no sharp and strong peak, but exhibits a broad peak at 20°, which proves the amorphous nature of PAGD.[23] These structures provide a favorable channel for the adsorption process, and through intermolecular interaction the dye molecules are well filled into these network structures. The zeta potential of the adsorbent PAGD was measured as shown in Fig. 1f and the results showed that the pH of solution may change the surface charge of PAGD and then influence its adsorption capacities. It can be seen that the point of zero charge (pH_{pzc}) values of the adsorbent PAGD was 4.5 ± 0.5. When the solution pH was lesser than pH_{pzc}, the adsorbent

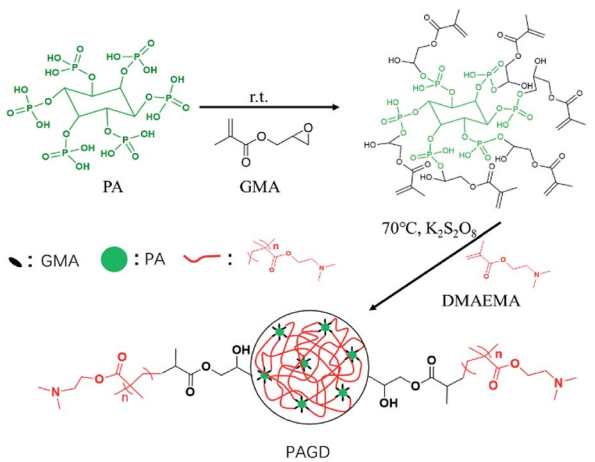

Scheme 1 Synthesis of PAGD.

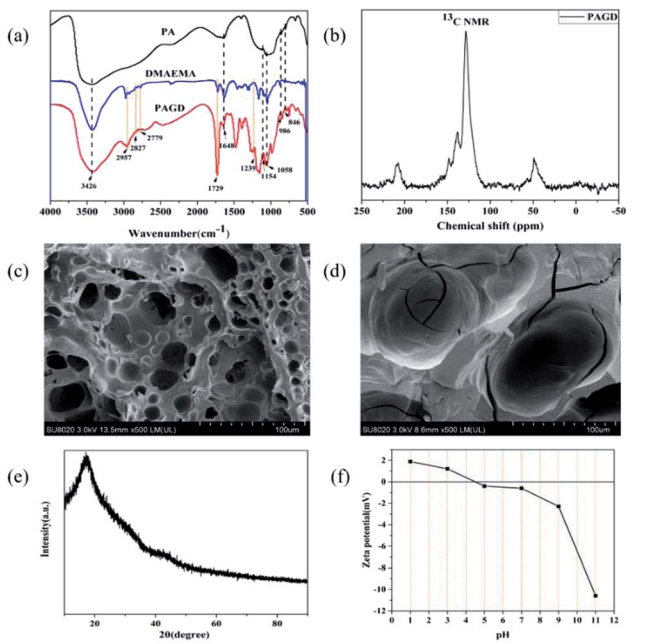

Fig. 1 FTIR spectra (a), solid-state ^{13}C NMR of PAGD (b), SEM section before adsorption (c), SEM section after adsorption (d) XRD (e) pattern of PAGD absorbent and zeta potential (f) of PAGD.

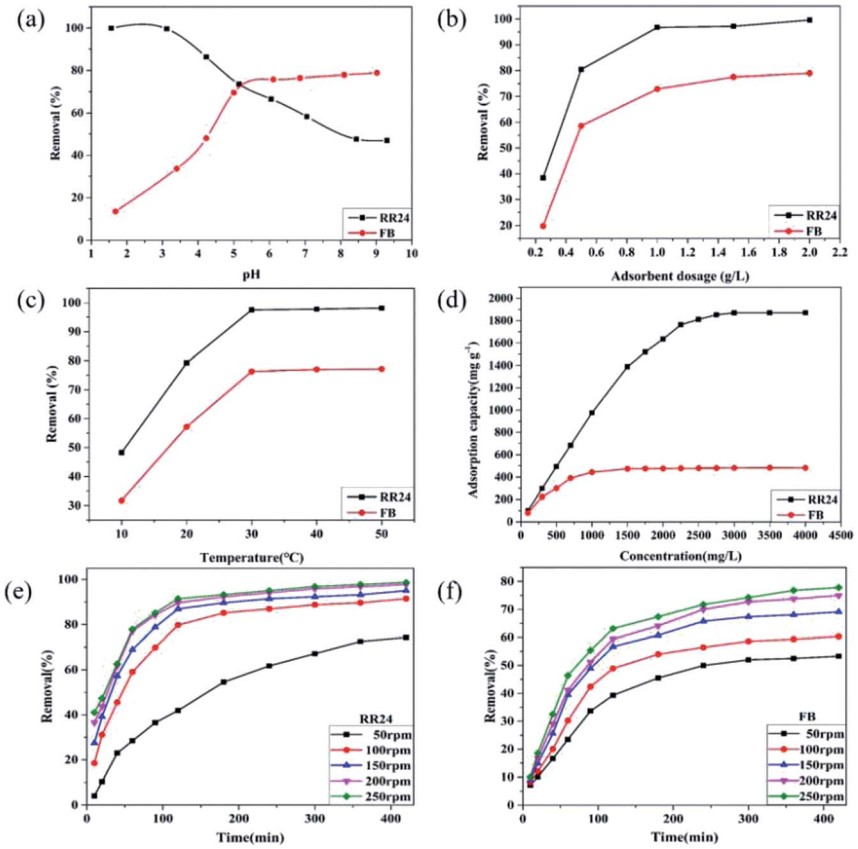

Fig. 2 Effect of pH value (a), adsorbent dosage of PAGD (b), temperature (c), dye concentration (d) and agitation speed ((e) and (f)) on adsorption of RR24 and FB.

PAGD showed positive electricity. On the contrary, it showed negative electricity when the solution pH was higher than pH_{pzc}.

3.2 Dye adsorption performances of the PAGD

3.2.1 Effect of dye solution pH on adsorption. RR24 (anionic dye) and FB (cationic dye) were elected as the dyes with which to investigate the adsorption behavior of PAGD. The influence of dye solution pH on PAGD adsorption is shown in Fig. 2a. The result reveals that the adsorption capacity of PAGD for RR24 dropped sharply from 99.91 to 47.61 mg g^{-1} and then stabilized with increasing pH. High adsorption at low pH values may be due to the tertiary amino groups in PAGD, which are ionized and interact with the dye molecules through strong electrostatic interactions.[33] At pH 3, the maximum removal rate of RR24 is over 99.59%. However, at high pH value, the $-PO_4^{3-}$ groups become dominant. The ionization degree of the H_3PO_4 group keeps increasing with increasing pH, which facilitates the adsorption of cationic dyes.[17] Therefore, the adsorption of FB increases as the pH increases and the maximum FB removal rate reaches more than 78.78% at pH 9.

Table 2 The adsorption capacity of different adsorbents towards RR24 and FB

Dye	Adsorbent	Adsorption efficiency (%)	Q_{max} (mg g^{-1})	References
RR24	PAGD	99.55	1871.23	This work
	MIL-101-Cr MOF	99	465	35
	Chitosan-metal	95.98	95.98	36
	Modified wheat straw	99.99	285.7	37
	Sludge-based activated carbon	94.68	34.46	38
	Activated carbon	—	23	39
FB	PAGD	73.12	482.54	This work
	Triptycene-based porous polymer grafted with sulfonic acid	99	586.2	40
	Biopolymer/ZSM-5 zeolite	81.2	237.5	41
	Fe(III) and Mn(II) modified activated carbons	99	238.1	42
	Graphene/beta-cyclodextrin	—	425.8	43

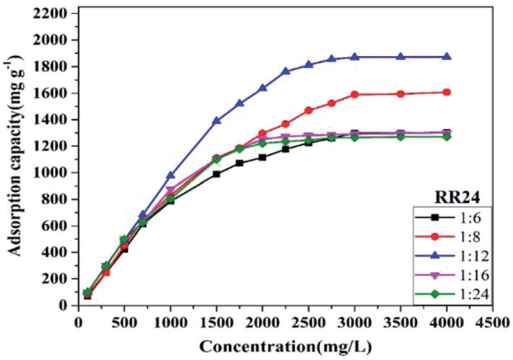

Fig. 3 Effect of molar ratio ([PA] : [DMAEMA] = 1 : 6, 1 : 8, 1 : 12, 1 : 16 and 1 : 24) on RR24 adsorption.

3.2.2 Effect of adsorbent dosage. To study how the dosage of adsorbent affects adsorption behavior, different contents of PAGD were used for adsorbing RR24 and FB, as shown in Fig. 2b. The percentage of dye removal improved with increased concentrations of adsorbent owing to the abundant effective active sites on PAGD adsorbents. When the dosage reaches 1.0 g L^{-1}, the adsorption becomes saturated and thus the removal efficiency reaches adsorption equilibrium. The removal efficiencies for RR24 and FB are 99.59% and 78.95%, respectively.

3.2.3 Effect of temperature. Dye adsorption was studied by varying temperatures from 10 °C to 50 °C. The dye-removal efficiency reveals significant growth with increasing temperature and then becomes stable at 30 °C, as shown in Fig. 2c. This result indicates that the relatively high temperature can promote dye adsorption and can be explained considering that dye molecules have increased mobility at high temperatures, and thus, more dyes can interact with PAGD. In addition, the active sites of PAGD interact with dye molecules having reached saturation when the temperature is above 30 °C.

3.2.4 Effect of dye concentrations. Fig. 2d reveals the influence of dye concentration on the adsorption process. The adsorption quantities of PAGD for RR24 and FB were probed at distinct concentrations from 100 to 4000 mg L^{-1}. First, as the dye concentration increases, the amount of adsorption is significantly enhanced. When the dye concentration is greater than a certain bound, the amount of adsorption increases until the equilibrium is reached. The maximum adsorption quantities (Q_{max}) of PAGD for RR24 and FB are 1871.23 and 482.54 mg g^{-1}, respectively. The adsorption abilities of different adsorbents for the removal of RR24 in this study and others are presented in Table 2. As can be seen from the table, the synthesized PAGD adsorbents exhibit superior adsorption capacity for RR24 compared to other previously reported adsorbents. The reasons for this phenomenon may be that, at low pH values, the introduced PA groups could act as a protonation agent under acid conditions and promote the protonation of tertiary amine groups in PAGD.[34] Moreover, since GMA-modified PA serves as cross-linking agent, the internal protonation of PAGD is further improved by interaction with PA, thus improving the adsorption of anionic dye.

3.2.5 Effect of agitation speed. In order to better optimize the experimental conditions, we did a batch experiment of dye adsorption with different speeds. From Fig. 2e and f we can see that when the stirring speed exceeds 100 rpm, the adsorption will quickly approach the adsorption equilibrium. With the increase of the stirring speed, the removal effect of the adsorbent PAGD on the two dyes is also obvious, but if the stirring speed exceeds 200 rpm, the removal effect of the adsorbent on the dye did not change much. The reason for the phenomenon may be that the contact area between the adsorbent and the dye has reached saturation.

To further investigate the effect of PA on the adsorption of anionic dye, different molar ratios of PA and DMAEMA were used to synthesize PAGD. As shown in Fig. 3, the Q_{max} value for RR24 increased significantly with increasing molar ratio below 1 : 12, due to the interaction between PA and DMAEMA, which promotes the internal protonation of PAGD. However, when the molar ratio is greater than 1 : 12, the protonation reaches saturation, and because of the decreased amount of DMAGMA, the Q_{max} value is decreased. This also indicates that PA enhances the adsorption of dyes by promoting the protonation effect of PAGD.

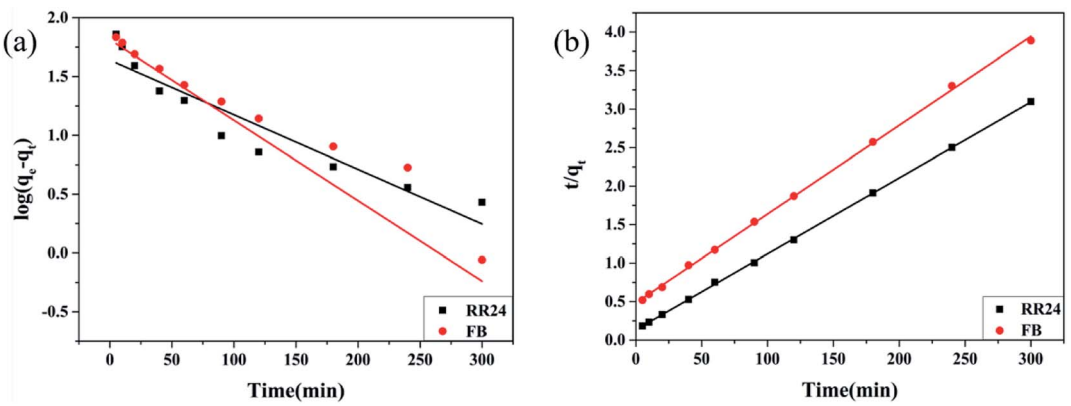

Fig. 4 The pseudo-first-order model (a) and pseudo-second-order model (b) for the removal of RR24 and FB.

Table 3 The kinetic parameters for RR24 and FB adsorption

		Pseudo-first-order model			Pseudo-second-order model			Intraparticle diffusion model		
Dyes	$(q_e)_{exp}$ (mg g^{-1})	$(q_e)_{cal}$ (mg g^{-1})	K_1 (min^{-1})	R^2	q_e (mg g^{-1})	$K_2 \times 10^{-3}$ (g mg^{-1} min^{-1})	R^2	C (mg g^{-1})	K_p (mg g^{-1} min$^{-1/2}$)	R^2
RR24	99.55	43.66	0.011	0.8829	101.42	0.73	0.9998	38.01	4.14	0.7587
FB	73.12	64.91	0.016	0.9795	74.13	0.26	0.9991	4.34	3.82	0.9361

3.3 Adsorption kinetics

In the kinetic experiments, 50 mg of adsorbent was mixed into a 50 mL aqueous dye solution (100 mg L^{-1}). For the purpose of investigating the adsorption mechanism and evaluating the adsorption efficiency of PAGD, pseudo-first-order[44] and pseudo-second-order kinetics,[45] which are described by eqn (4) and (5), respectively, served to fit the experimental data:

$$\log(q_e - q_t) = \log(q_e) - \frac{K_1}{2.303}t \quad (4)$$

$$\frac{t}{q_t} = \frac{1}{K_2 q_e^2} + \frac{t}{q_e} \quad (5)$$

where K_1 and K_2 are the rate constants of pseudo-first-order and pseudo-second-order kinetics; q_e and q_t (mg g^{-1}) represent the absorbability of adsorbent at balanced contact time and t (min), respectively.

The comparison of results and fitting lines are presented in Fig. 4, and the kinetic parameters listed in Table 3. It is apparent that the R^2 value of pseudo-second-order kinetics (0.9995) is better than that of pseudo-first-order kinetics (0.9666). In addition, the adsorption quantities (Q_e) of pseudo-second-order kinetics for RR24 and FB are 99.55 and 73.12 mg g^{-1}, respectively, which are in close proximity to the respective laboratory Q_e values (101.42 and 74.13 mg g^{-1}). From the results above, the pseudo-second-order model could be a better description of the adsorption course to RR24 and FB. It reveals that the intensity of ionic interplay is excellent among the adsorbent and the dyes[46] and the mechanism of adsorb the dyes by the adsorbent could be depicted in Fig. 5, which is consistent with the effect of pH in Section 3.2.1.

The process of adsorption is studied thoroughly by means of the intraparticle diffusion model[47] and the model is described by eqn (6):

$$q_t = K_p(t^{1/2}) + C \quad (6)$$

where q_t (mg g^{-1}) is the absorbability of adsorbent at time t (min), the rate constant of the intraparticle diffusion model is expressed by K_p, and C (mg g^{-1}) represents a constant involving the thickness and boundary layer. Adsorption equilibrium is reached within 120 min, and adsorption quantities for RR24

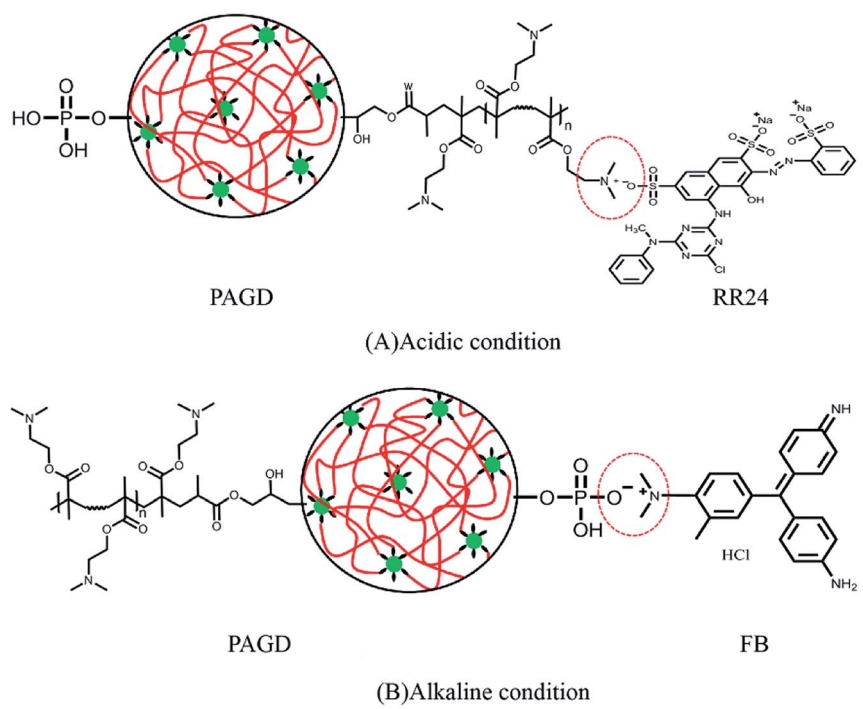

Fig. 5 The adsorb mechanism of adsorb the RR24 (A) and FB (B) by PAGD.

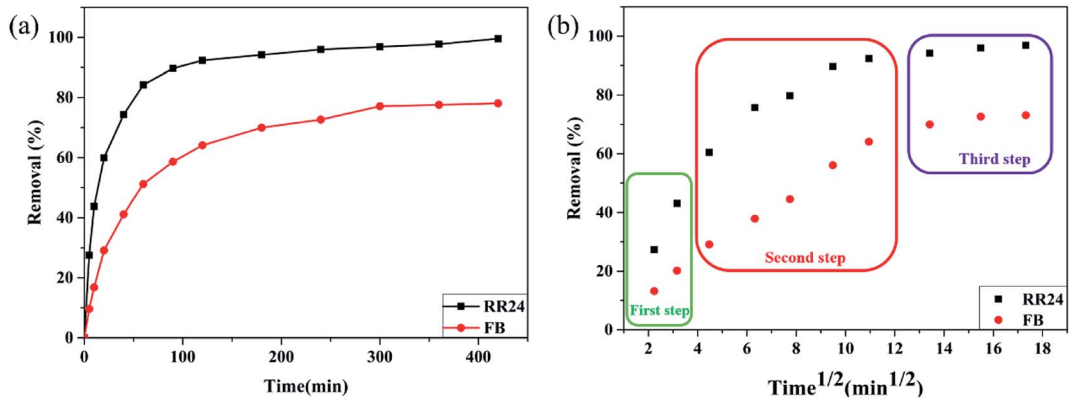

Fig. 6 Contact time (a) and plot of q_t values *versus* $t^{1/2}$ (b) for the adsorption of RR24 and FB.

and FB up to 90 and 60 mg g^{-1} are obtained for PAGD, respectively (Fig. 6a). As shown in Fig. 6b, the adsorbent process of PAGD adsorbent on dye is basically related to three subsequent steps, as follows: The first step reveals the adsorption on the surface or a transient adsorption process; the second step is the increasing adsorption process, which comprises the rate-controlled steps of intra-particle diffusion; and the third step is the adsorption balance course, where the rate of the intra-particle diffusion decreases as a result of excessively rare concentration of dyes.[48]

3.4 Adsorption isotherms

The equilibrium adsorption isotherm plays an important role in the investigation of the adsorption mechanism. In Fig. 2a, the optimal adsorption capacity onto PAGD occurred at pH 3.0 and 9.0 for RR24 and FB, respectively. Thus, the research on adsorption equilibrium was carried out under appropriate pH values. The adsorption isotherms of PAGD on RR24 and FB with the corresponding concentrations and temperatures are shown in Fig. 2c and d, respectively. In addition, essential information for studying the suitability of the adsorption course is furnished by the adsorption equilibrium. Langmuir, Freundlich, and Temkin isotherm models are used to depict the adsorption mechanism.

The Langmuir isotherm model[49] is frequently used in determining the monolayer adsorption equilibrium, which can be expressed as eqn (7):

$$\frac{C_e}{q_e} = \frac{1}{q_m K_L} + \frac{C_e}{q_m} \quad (7)$$

where q_e (mg g^{-1}) and q_{max} (mg g^{-1}) are the adsorption capacities at the balanced and maximum times, respectively. C_e (mg L^{-1}) is the equilibrium concentration of dye and K_L (L mg^{-1}) the Langmuir constant of the reaction rate.

The Freundlich isotherm model[50] is an empirical model for modeling heterogeneous systems on adsorbent surfaces, which assumes a heterogeneous distribution of absorbent surfaces and multimolecular layer adsorption. The Freundlich isotherm model is expressed by eqn (8):

$$\log q_e = \log K_F + \frac{1}{n} \log C_e \quad (8)$$

where q_e (mg g^{-1}) is the equilibrium adsorption capacity, C_e (mg L^{-1}) the dye concentration, and K_f (L mg^{-1}) and n are rate constants and the adsorption strength of the Freundlich model, respectively.

The Temkin isotherm model is also used to calculate the adsorption of heterogeneous systems.[51] The Temkin isotherm assumes that the adsorption binding energy can be evenly distributed and the heat of adsorption reduced as the

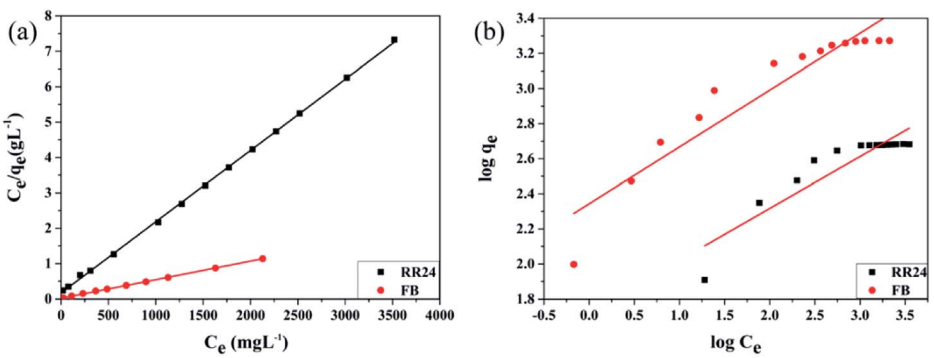

Fig. 7 Langmuir (a) and Freundlich (b) adsorption isotherm of PAGD for RR24 and FB.

Table 4 Isotherm date of PAGD for RR24 and FB adsorption

		Langmuir isotherm			Freundlich isotherm			Temkin isotherm		
Dyes	Q_{max} (mg g^{-1})	(Q_e) (mg g^{-1})	K_L (L mg^{-1})	R^2	n	K_F (mg L^{-1})	R^2	A (L mg^{-1})	d (J mol^{-1})	R^2
RR24	1871.23	1900.05	0.032	0.9995	3.09	220.41	0.8827	1.586	10.089	0.9794
FB	482.54	497.51	0.012	0.9996	3.38	53.05	0.8249	3.771	32.626	0.9217

interaction between PAGD and dye is enhanced. The Temkin model is described by eqn (9):

$$\ln q_e = \frac{RT}{d} \ln(AC_e) \quad (9)$$

and the relationship is linear according to eqn (10):

$$q_e = B \ln A + B \ln C_e \quad (10)$$

where q_e (mg g^{-1}) is the equilibrium adsorption capacity; R (8.314 J mol^{-1} K^{-1}) is the conventional gas constant and T (K) is the absolute reaction temperature; $B = RT/d$; C_e (mg L^{-1}) is the concentration of dye; A (L mg^{-1}) and d (J mol^{-1}) are the Temkin constants of reaction rate, respectively. The fitting linear relationship is demonstrated in Fig. 7 and the isotherm arguments are aggregated in Table 4.

The result of the relative parameter values can be obtained from Table 4, which is derived from the Langmuir, Freundlich, and Temkin isotherms. The extreme theoretical extent of adsorption for RR24 and FB is 1900.05 and 497.51 mg g^{-1}, respectively, which is near the true-experimental research values for RR24 and FB (1871.23 and 482.54 mg g^{-1}, respectively). K_L expresses the rate constants of the Langmuir model and the values range from 0 to 1, indicating that the adsorbent is beneficial for adsorbing two dyes. The values of K_F indicate that PAGD is appropriate for adsorption of RR24 and FB, and its values show the ease of adsorption onto the two dyes and, further, that the adsorption ability increases with increasing dye concentration. The rate constants n of the Freundlich model illustrates the advantage and capacity of the adsorption, and $n > 1$ verifies it as a beneficial adsorption system. The high d values of the Temkin model reveal the powerful interaction between PAGD and dyes. Consequently, the R^2 value of the Langmuir model is higher than that of both the Freundlich and Temkin isotherm models, because the process of absorbing RR24 and FB on PAGD is monolayer adsorption.[52]

3.5 Separation property of dye mixture

Since there is some interaction between anionic and cationic dyes, which is difficult to remove, we studied the separation of anionic–cationic mixed dye, which facilitates the separation and reproducibility of the dye for use in other aspects. PAGD exhibits excellent adsorption properties for the anionic dye RR24 when the solution is in an acid condition. To evaluate the separation property of a dye mixture, a mixed solution of anionic and cationic dyes was prepared at a molar ratio of 1 : 1. As shown in Fig. 8a, the maximum peaks of RR24 and FB are 533 and 543 nm, respectively, while the mixed solution only shows the largest peak at 533 nm (Fig. 8a). This phenomenon may be due to the electrostatic attraction that leads to the combination of RR24 and FB in water solution (Fig. 9a). After adsorption of

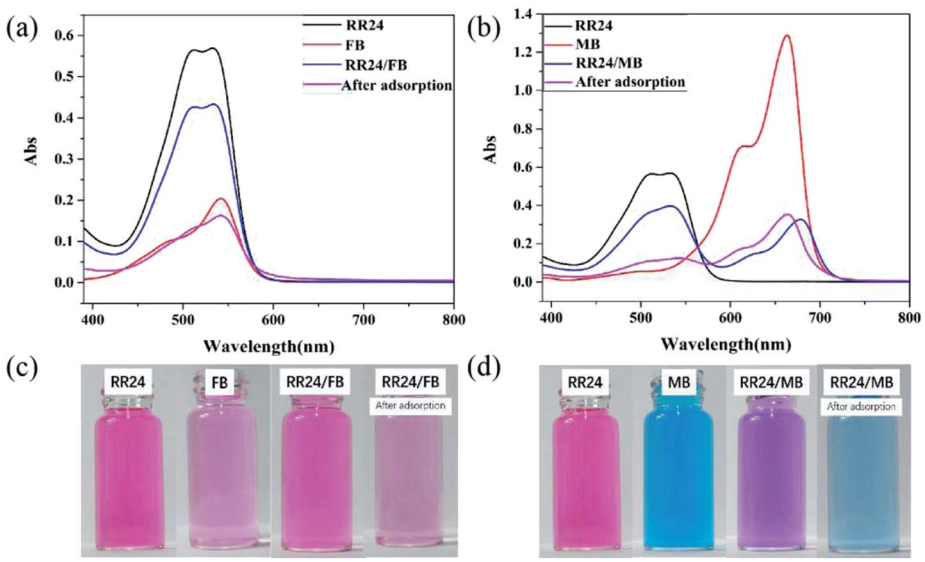

Fig. 8 The UV-vis spectra of RR24/FB (a), the UV-vis spectra of RR24/MB (b), the image of RR24/FB (c) and the image of RR24/FB (d).

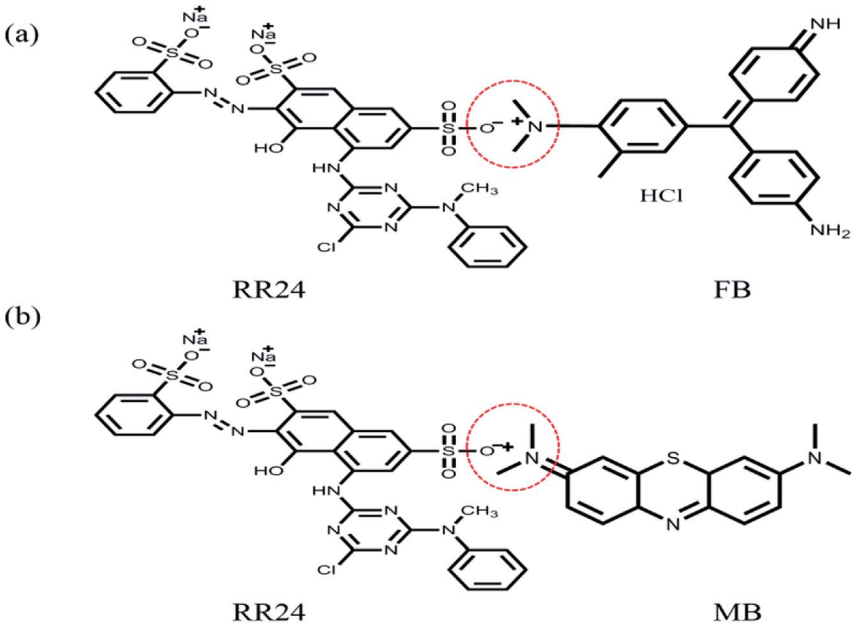

Fig. 9 The interaction between RR24 and cationic dyes of FB (a) or MB (b).

the dye mixture with PAGD, the spectrum is close to the spectrum of FB, and the color changes from light red to pale pink, indicating that the anionic dye RR24 is selectively separated from the mixed dye (Fig. 8c).

To further study the separation ability of PAGD for separation between RR24 and anionic dye, we performed a separation experiment of mixed dyes of RR24 and MB (Fig. 8b). The maximum absorption wavelength of MB is shifted from 664 to 680 nm, and the mixed MB peak is much lower than the MB peak due to the interaction between MB and RR24 (Fig. 9b). Since RR24 is selectively adsorbed after the adsorption of the dye mixture, the maximum absorption wavelength of MB is transferred to 664 nm, and the absorption spectrum of RR24 is close to zero after adsorption (Fig. 8b). Moreover, the mixer color, which changed from purple to blue (Fig. 8d), suggests that PAGD can effectively separate RR24 and MB.

3.6 Desorption and recycle

Based on the above discussion, ionic interaction is known to be dominant in dye adsorption by PAGD, and thus, we can command the quantity of cationic and anionic functional groups of PAGD by transferring the pH value. Then, the desorption experiment of the cationic dye FB is primarily carried out under acidic conditions. Since the negative $-PO_4^{3-}$ group is protonated by H^+, the electrostatic attraction between the adsorbent surface and FB cationic dye is reduced. Moreover, the repulsive strength in the middle of FB and PAGD may be improved under an acid medium with the protonation of tertiary amine. Desorbing FB from the adsorbent at pH 3 is shown in Fig. 10a. More than 71.56% of the FB can be stripped within 300 min, evidencing the higher-efficiency property of the desorption abilities of PAGD. With regard to the anionic dye RR24, the desorption was fulfilled at pH 11. For the reason that the increased amount of deprotonated $-PO_4^{3-}$ groups reduces

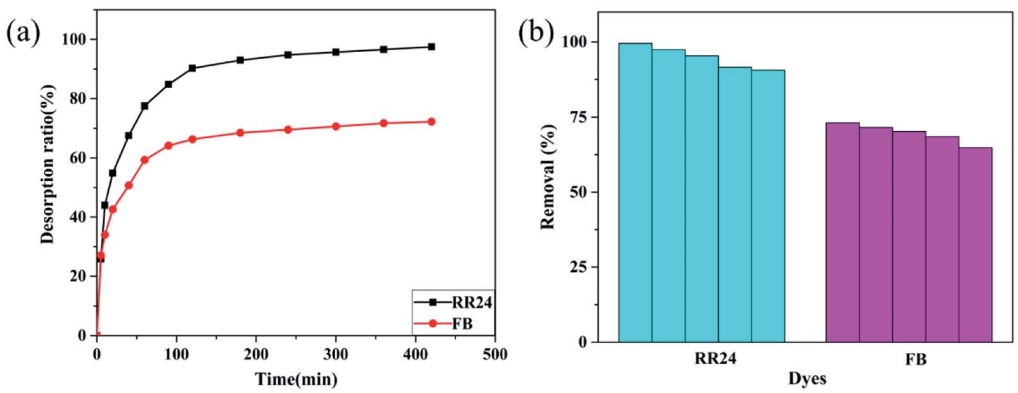

Fig. 10 Desorption (a) and recycle (b) performance of PAGD for RR24 and FB.

the interaction between the adsorbent surface and the anionic dye, 97.36% of the RR24 could be striped. These results indicate that PAGD has excellent invertibility for dye adsorption and desorption.

The recycle of PAGD was studied by performing adsorption–desorption cycles for five times. PAGD retains high removal efficiency for RR24 (90.58–99.55 mg g^{-1}) and FB (64.82–73.12 mg g^{-1}) as shown in Fig. 10b, suggesting that PAGD is a reusable absorbent.

4. Conclusions

The effective PAGD adsorbent was successfully synthesized from PA, GMA, and DMAEMA, which exhibits pH-sensitive adsorption performance of two dyes. PAGD demonstrates outstanding adsorbability on anionic dye RR24 at pH 3, and the maximum adsorption capacity is 1871.23 mg g^{-1}. Moreover, PAGD could effectively adsorb the cationic dye FB at pH 9, for which the maximum adsorption capacity is 482.54 mg g^{-1}. The process of desorption was accomplished under basic (pH 11) for RR24 or acidic (pH 3) conditions for FB, and more than 97.36% of the RR24 and 71.56% of the FB can be desorbed. The separation property of the dye mixture indicated that PAGD could effectively remove RR24 in cationic dye/RR24 mixed solutions. In addition, the adsorption process of dyes aided by the pseudo-second-order model and Langmuir mono-layer adsorption and its results correlate well. PAGD can be reused as a new adsorbent, and its adsorption capacity reserved at over 89% through five adsorption–desorption cycles. Therefore, PAGD can serve as a potential material for the removal of synthetic dyes from wastewater, and continued investigation could discover other application scenarios.

Conflicts of interest

There are no conflicts to declare.

Acknowledgements

This work was supported by the National Natural Science Foundation of China (21467024, 21661027 and 51764049), high-level talent start-up capital of Shihezi University (RCZX201509) and the opening project of the key laboratory for green processing of chemical engineering of Xinjiang Bingtuan (KF201703).

References

1 M. T. Yagub, T. K Sen, S. Afroze and H. M. Ang, *Adv. Colloid Interface Sci.*, 2014, **209**, 172–184.
2 M. Ahmad, M. Yousaf, A. Nasir, I. A. Bhatti, A. Mahmood, X. C. Fang, X. Jian, K. Kalantar-Zadeh and N. Mahmood, *Environ. Sci. Technol.*, 2019, **53**, 2161–2170.
3 Y. Fan, H. J. Liu, Y. Zhang and Y. Chen, *J. Hazard. Mater.*, 2015, **283**, 321–328.
4 D. Jiang, M. Chen, H. Wang, G. M. Zeng, D. L. Huang, M. Cheng, Y. Liu, W. J. Xue and Z. W. Wang, *Coord. Chem. Rev.*, 2019, **380**, 471–483.
5 C. Li, J. Cui, F. Wang, W. Peng and Y. He, *Desalin. Water Treat.*, 2016, **57**, 14060–14066.
6 Y. Tian, B. Ju, S. Zhang and L. Hou, *Carbohydr. Polym.*, 2016, **136**, 1209–1217.
7 Z. H. Huang, Y. Z. Li, W. J. Chen, J. H. Shi, N. Zhang, X. J. Wang, Z. Li, L. Z. Gao and Y. X. Zhang, *Mater. Chem. Phys.*, 2017, **202**, 266–276.
8 V. Katheresan, J. Kansedo and S. Y. Lau, *J. Environ. Chem. Eng.*, 2018, **6**, 4676–4697.
9 P. Kaur, V. K. Sangal and J. P. Kushwaha, *Int. J. Environ. Sci. Technol.*, 2019, **16**, 801–810.
10 J. Vidal, L. Villegas, J. M. Peralta-Hernández and R. Salazar González, *J. Environ. Sci. Health, Part A: Toxic/Hazard. Subst. Environ. Eng.*, 2016, **51**, 289–296.
11 A. Salama, *J. Colloid Interface Sci.*, 2017, **487**, 348–353.
12 M. S. U Rehman, I. Kim and J. I. Han, *Carbohydr. Polym.*, 2012, **90**, 1314–1322.
13 J. W. Fu, Q. Q. Xin, X. C. Wu, Z. H. Chen, Y. Yan, S. J. Liu, M. H. Wang and Q. Xu, *J. Colloid Interface Sci.*, 2016, **461**, 292–304.
14 H. Hadi Alkarawi and G. Zotz, *Plant Biol.*, 2014, **16**, 697–701.
15 X. H. Song, Y. Y. Chen, M. C. Rong, Z. X. Xie, T. T. Zhao, Y. R. Wang, X. Chen and O. S. Wolfbeis, *Angew. Chem., Int. Ed.*, 2016, **55**, 3936–3941.
16 K. Cai, W. Shen, B. Ren, J. He, S. Wu and W. Wang, *Chem. Eng. J.*, 2017, **330**, 936–946.
17 Z. Zhao, L. L. Li, G. S. Geleta, L. Ma and Z. X. Wang, *Sci. Rep.*, 2017, **7**, 7878.
18 H. You, J. C. Chen, C. Yang and L. Q. Xu, *Colloids Surf., A*, 2016, **509**, 91–98.
19 A. Salama, N. Shukry and M. El-Sakhawy, *Int. J. Biol. Macromol.*, 2015, **73**, 72–75.
20 J. S. Karthika and B. Vishalakshi, *Int. J. Biol. Macromol.*, 2015, **81**, 648–655.
21 P. B. Krishnappa and V. Badalamoole, *Int. J. Biol. Macromol.*, 2019, **122**, 997–1007.
22 M. M. Liu, L. Z. Zhao, S. S. Li, H. Ye, H. Q. An and Y. Z. Zhang, *RSC Adv.*, 2016, **6**, 10704–10712.
23 A. M. Goganian, N. Arsalani, H. K. Khiabani and M. S. Zakerhamidi, *J. Polym. Res.*, 2014, **21**, 484.
24 F. Carosio, G. Fontaine, J. Alongi and S. Bourbigot, *ACS Appl. Mater. Interfaces*, 2015, **7**, 12158–12167.
25 F. Razmjooei, K. P. Singh, E. J. Bae and J. S. Yu, *J. Mater. Chem. A*, 2015, **3**, 11031–11039.
26 X. Guo, Y. Miao, P. Ye, Y. Wen and H. Yang, *Mater. Res. Express*, 2014, **1**, 025403.
27 G. Jiang, J. Qiao and F. Hong, *Int. J. Hydrogen Energy*, 2012, **37**, 9182–9192.
28 M. Zhao, C. Deng and X. Zhang, *ACS Appl. Mater. Interfaces*, 2013, **5**, 13104–13112.
29 Z. G. Wang, X. L. Fan, M. He, Z. Q. Chen, Y. F. Wang, Q. F. Ye, H. J. Zhang and L. Zhang, *J. Mater. Chem. B*, 2014, **2**, 7559–7566.

30 M. F. Xia, W. C. Lang, Y. Yang, J. H. Yu, N. J. Wu and Q. G. Wang, *Materials*, 2019, **12**, 294.
31 J. Park, Q. Ye, P. Spencer and J. S. Laurence, *Int. J. Polym. Mater.*, 2012, **61**, 144–153.
32 H. Y. Li, B. Meng, S. H. Chai, H. L. Liu and S. Da, *Chem. Sci.*, 2016, **7**, 905–909.
33 Y. X. Wang, L. Y. Zhao, H. L. Peng, J. N. Wu, Z. Y. Liu and X. H. Guo, *J. Chem. Eng. Data*, 2016, **61**, 3266–3276.
34 J. W. Ji, R. Li, H. Y. Li, Y. Shu, Y. Li, S. Q. Qiu, C. Q. He and Y. K. Yang, *Composites, Part B*, 2018, **155**, 132–137.
35 S. Karmakar, D. Roy, C. Janiak and S. De, *Sep. Purif. Technol.*, 2019, **215**, 259–275.
36 H. Zhou, L. Xu, Y. Wen, K. Lin and X. Zeng, *J. Colloid Interface Sci.*, 2017, **490**, 233–241.
37 X. Xu, B. Y. Gao, Q. Y. Yue and Q. Q. Zhong, *J. Hazard. Mater.*, 2010, **182**, 1–9.
38 W. H. Li, Q. Y. Yue, B. Y. Gao, Z. H. Ma, Y. J. Li and H. X. Zhao, *Chem. Eng. J.*, 2011, **171**, 320–327.
39 Q. Y. Yue, J. K. Xie, B. Y. Gao, H. Yu, W. W. Yue, X. S. Zhang and X. N. Wang, *Acta Sci. Circumstantiae*, 2007, **27**, 1431–1438.
40 C. Li, Y. He, L. Zhou, T. Xu, J. Hu, C. J. Peng and H. L. Liu, *RSC Adv.*, 2018, **8**, 41986–41993.
41 G. V. Brião, S. L. Jahn, E. L. Foletto and G. L. Dotto, *Colloids Surf., A*, 2018, **556**, 43–50.
42 L. H. Huang, J. J. Kong, W. L. Wang, C. L. Zhang, S. F. Niu and B. Y. Gao, *Desalination*, 2012, **286**, 268–276.
43 P. Tan and Y. Hu, *J. Mol. Liq.*, 2017, **242**, 181–189.
44 S. Lagergren and K. Sven, *Vetenskapsakad. Handl. Band.*, 1898, vol. 24, pp. 1–39.
45 Y. S. Ho and G. McKay, *Process Biochem.*, 1999, **34**, 451–465.
46 Y. Fan, H. J. Liu, Y. Zhang and Y. Chen, *J. Hazard. Mater.*, 2015, **283**, 321–328.
47 W. J. Weber and J. C. Morris, *J. Sanit. Eng. Div., Am. Soc. Civ. Eng.*, 1963, **89**, 31–60.
48 J. Zhang, Q. Zhou and L. Ou, *J. Chem. Eng. Data*, 2012, **57**, 412–419.
49 I. Langmuir, *J. Am. Chem. Soc.*, 1916, **38**, 2221–2295.
50 H. Freundlich, *Z. Phys. Chem.*, 1907, **57**, 385–470.
51 M. J. V. Temkin, *Acta Physicochim. URSS*, 1940, **12**, 217–222.
52 L. Liu, Z. Y. Gao, X. P. Su, X. Chen, L. Jiang and J. M. Yao, *ACS Sustainable Chem. Eng.*, 2015, **3**, 432–442.

